

Title	Image based Particle Shape Analysis Toolbox (IPSAT)
Authors	Tunwal, Mohit;Mulchrone, Kieran F.;Meere, Patrick A.
Publication date	2019-11-26
Original Citation	Tunwal, M., Mulchrone, K. F. and Meere, P. A. (2020) 'Image based Particle Shape Analysis Toolbox (IPSAT)', Computers & Geosciences, 135, 104391, (11 pp). doi: 10.1016/j.cageo.2019.104391
Type of publication	Article (peer-reviewed)
Link to publisher's version	https://www.sciencedirect.com/science/article/pii/S0098300419305771 - 10.1016/j.cageo.2019.104391
Rights	© 2019 Elsevier Ltd. All rights reserved. This manuscript version is made available under the CC BY-NC-ND 4.0 license.
Download date	2024-05-01 01:49:19
Item downloaded from	https://hdl.handle.net/10468/9794



UCC

University College Cork, Ireland
 Coláiste na hOllscoile Corcaigh

Journal Pre-proof

Image based Particle Shape Analysis Toolbox (IPSAT)

Mohit Tunwal, Kieran F. Mulchrone, Patrick A. Meere

PII: S0098-3004(19)30577-1

DOI: <https://doi.org/10.1016/j.cageo.2019.104391>

Reference: CAGEO 104391

To appear in: *Computers and Geosciences*

Received Date: 10 June 2019

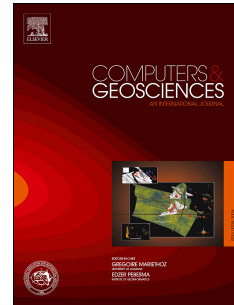
Revised Date: 22 November 2019

Accepted Date: 24 November 2019

Please cite this article as: Tunwal, M., Mulchrone, K.F., Meere, P.A., Image based Particle Shape Analysis Toolbox (IPSAT), *Computers and Geosciences* (2019), doi: <https://doi.org/10.1016/j.cageo.2019.104391>.

This is a PDF file of an article that has undergone enhancements after acceptance, such as the addition of a cover page and metadata, and formatting for readability, but it is not yet the definitive version of record. This version will undergo additional copyediting, typesetting and review before it is published in its final form, but we are providing this version to give early visibility of the article. Please note that, during the production process, errors may be discovered which could affect the content, and all legal disclaimers that apply to the journal pertain.

© 2019 Published by Elsevier Ltd.



1 **Image based Particle Shape Analysis Toolbox (IPSAT)**

2 *Mohit Tunwal¹⁾²⁾*, Kieran F. Mulchrone²⁾ and Patrick A. Meere¹⁾*

3 *¹⁾ School of Biological, Earth and Environmental Sciences, University College Cork, Distillery*
4 *Fields, North Mall, Cork, T23 TK30, Ireland*

5 *²⁾School of Mathematical Sciences, University College Cork, Western Gateway Building,*
6 *Western Road, Cork, T12 XF62, Ireland*

7 ***Corresponding Author:** Mohit Tunwal¹

8 **Contact:** mohittunwal@gmail.com; mohit.tunwal@ucc.ie; +353-21-490-4580

9 **Link to code:** <https://github.com/tunwalm/IPSAT>

10

11 **Highlights:**

- 12 • Image analysis toolbox for particle shape and size analysis is presented
- 13 • 12 shape and 6 size parameters are available in the toolbox
- 14 • 2D to 3D size transformation & data visualisation tools are present in the toolbox
- 15 • Methodology for both loose as well as compacted samples is proposed
- 16 • Toolbox offers a cheap, fast and robust method for quantitative textural analysis

¹¹ Authorship Statement: MT and KFM developed the code. MT, KFM and PAM conceptualised the study as well as contributed to drafting the manuscript.

17 Abstract

18 Shape analysis can provide vital information regarding the origin, transport and deposition
19 history of grains. Particle shape measurement has been an active area of research for
20 sedimentologists since the 20th century. With advancement in the field of computation and
21 image analysis, shape analysis can be done in a faster and much more accurate way compared to
22 manual measurements. The results obtained are reproducible as compared to visual qualitative
23 analysis. However, there is a lack of image analysis software tools aimed at the field of
24 sedimentology where the fine details of a particle boundaries are required. Image based Particle
25 Shape Analysis Toolbox (IPSAT) developed in the Mathematica environment for the
26 quantitative characterisation of sedimentary grains in 2-dimensions is presented here. This image
27 analysis toolbox can be used to analyse consolidated as well as loose sediment samples. A total
28 of 12 parameters are available for shape measurement comprising conventional shape parameters
29 (roundness, angularity, circularity and irregularity), mathematically complex shape parameters
30 (fractal dimension and Fourier descriptors) and common geometrical shape parameters (aspect
31 ratio, convexity, solidity, mod ratio, rectangularity and compactness). Additionally, IPSAT offers
32 to compute 6 particle size measurement parameters. Furthermore, 2-D particle size distribution
33 can be transformed to a 3-D size distribution for thin section analysis. Example analyses have
34 been carried out on a sandstone and a loose sediment sample. The toolbox presented here aims to
35 establish a textural analysis methodology to be used by geologists and sedimentologists in
36 particular. It will allow users to quantitatively characterise a large set of grains with a fast, cheap
37 and robust methodology.

38

39 Keywords: particle shape, particle size, image analysis, texture, roundness, angularity

40 1. Introduction

41 Particle shape analysis is of interest to a wide range of fields in geology such as igneous and
42 metamorphic petrology (Higgins, 2006), structural geology (Heilbronner and Barrett, 2014;
43 Mulchrone et al., 2013), volcanology (Charpentier et al., 2013; Sarocchi et al., 2011), and
44 sedimentology (Blott and Pye, 2008). Shape analysis of sedimentary particles has occupied
45 sedimentologists for over a century (Barrett, 1980; Blott and Pye, 2008 and references therein) as
46 it provides vital information regarding the origin, transport and deposition history (Pettijohn,
47 1957). However, shape analysis studies suffer from two common shortcomings: 1) with a
48 plethora of available shape parameters, a standardised methodology is lacking; 2) most of these
49 shape parameters are time consuming and tedious to calculate manually. Visual comparison
50 charts were proposed to ease the effort required for shape analysis (Krumbein, 1941; Powers,
51 1953). However, qualitative comparison methods suffer from user bias and reproducibility issues
52 (Blatt, 1992; Blatt et al., 1972).

53 In recent years, with the advancement of computational power and image analysis techniques,
54 shape analysis has received a renewed focus (Campaña et al., 2016; Moreno Chávez et al., 2018;
55 Eamer et al., 2017; Lira and Pina, 2009; Sochan et al., 2015; Suzuki et al., 2015; Tao et al.,
56 2018). Most of these methods have been primarily applied to loose sediments where it is easier
57 to define grain boundaries automatically. On the other hand, the currently available automated
58 grain boundary segmentation algorithms (Calderon De Anda et al., 2005; Gorsevski et al., 2012;
59 Li et al., 2008; Mingireanov Filho et al., 2013; Roy Choudhury et al., 2006) do not produce the
60 quality of grain boundary data from thin section microphotographs typically required for shape
61 analysis. A high resolution microphotograph with clear distinction between matrix and clasts is

62 usually required (Roduit, 2007) for such automated grain boundary segmentation but this is the
63 exception rather than the rule.

64 Another shortcoming in presently available image analysis tools is that they do not offer a wide
65 range of shape parameters for a comprehensive shape analysis study. One of the most widely
66 used image analysis software platforms, ImageJ, was developed primarily for use by biologists
67 (Schneider et al., 2012). Hence, the *shape descriptors* present are basic geometrical shape
68 measures related to overall macro features of the particle shape rather than a detailed
69 characterisation of the particle outline as required for example for roundness measurement.
70 Furthermore, recently proposed shape parameters by various researchers are either conceptual
71 (Takashimizu and Iiyoshi, 2016) or are presented in standalone software (Charpentier et al.,
72 2013; Heilbronner and Barrett, 2014).

73 The aim of this contribution is to present Image based Particle Shape Analysis Toolbox (IPSAT)
74 – an image analysis software package that offers a wide range of shape and size parameters.
75 IPSAT can used to quantitatively analyse particles from both loose sediments and rock thin
76 section microphotographs. In the case of loose sediments, a fully automated approach is
77 presented. On the other hand, manual tracing of grain boundaries is suggested for thin section
78 photomicrographs. IPSAT is developed on the Mathematica platform which offers a variety of
79 in-built powerful image analysis and computational routines.

80 The implementation details of the software code along with details of textural parameters are
81 described in the next section. Example analyses for both loose and consolidated sediments are
82 provided. The image analysis toolbox presented in this paper aims to establish a methodology for
83 reproducible and comparable quantitative textural analysis of particles.

84 2. Software description

85 Mathematica is used as the basis for IPSAT and is a powerful technical computing environment
86 with an excellent array of features and applications that run on a variety of operating systems
87 such as Windows, Mac OS and Linux (Trott, 2013; Wellin et al., 2005). The IPSAT code is
88 wrapped up in a single Mathematica package. Additionally, two example Mathematica
89 notebooks are provided demonstrating the analysis of a thin section and a loose sediment sample.
90 These notebooks guide the user through the procedure, i.e. from image import to image analysis,
91 feature extraction, and computation of all the textural parameters. Furthermore, a detailed user
92 manual is also included which provides step-by-step guide for usage of functions described in
93 this section. The functionality of IPSAT package is summarised in Figure 1, the implementation
94 details of which are as follows:

95 2.1. Image input and analysis

96 If a sample of unconsolidated (loose) sediment is to be analysed, then the process is much
97 simpler and fully automated. Particles are recommended to be setup on the stage such that they
98 do not touch each other (see Fig. 2a). In case of image from transmitted light, the background is
99 expected to be light coloured with exceptions of dark region(s) representing particle(s). On the
100 other hand, a black background with contrasting light coloured region(s) containing particle(s) is
101 recommended for reflected light source image. The input image for loose sediment can be of any
102 standard image format (e.g., JPEG, TIFF, PNG).

103 In the case of particles from lithified samples such as sandstone, photomicrographs of thin
104 sections are used. Manual tracing of particle boundaries is performed because automated image
105 analysis techniques are not yet satisfactory (Moreno Chávez et al., 2015; Gorsevski et al., 2012;

106 Li et al., 2008; Mingireanov Filho et al., 2013; Roy Choudhury et al., 2006). It is recommended
107 that tracing paper and black inking pens are used for tracing (Mulchrone et al., 2013) or,
108 alternatively, a graphics tablets may be used. Images consisting of black boundaries on a white
109 background are the required input for the software (see Fig. 3b). A bitmap file (BMP) is
110 recommended to be used as input for the manually traced image. Further details on image
111 acquisition is provided in the Example Analysis (see section 3).

112 The **GrainBoundary** function is present only in the loose sediment analysis notebook. It detects
113 the particle boundary using a threshold which can be changed, if required, by the user. The
114 output of this step generates an image similar to a manually traced image (see Fig. 2b). All
115 subsequent steps are same for both loose sediment and thin section image analysis.

116 Two functions (**GrabImage** and **RefineImage**) are written for image analysis purposes. The
117 **GrabImage** function directly takes manually traced input image in the case of thin section
118 analysis. For loose sediment analysis, the output of **GrainBoundary** is used as the input for the
119 **GrabImage** function. **GrabImage** performs the following tasks:

- 120 (i) converts the input image into a binary image
- 121 (ii) generates a matrix by applying the watershed transformation on the image from step (i), at
122 this stage all the particles are separately identified
- 123 (iii) using the built-in Mathematica function (ComponentMeasurement), all the initial geometric
124 information regarding the grains are computed – long and short axis of best fit ellipse,
125 orientation, centroid, area, convex area, perimeter and convex perimeter.

126 After the **GrabImage** function runs, it outputs a coloured image displaying individual particle
127 regions in different colours with a unique label number (see Fig. 2c and 3c). Erroneous

128 identifications may remain at this point, where boundaries of neighbouring particles meet and
129 form a closed loop.

130 **RefineImage** is a function allowing users to remove any erroneously identified regions. It
131 accepts as an argument a list of the labels of unacceptable particles and removes them from
132 further processing. Once RefineImage is run, a revised colourised image of identified particle
133 regions is presented. This step may be repeated until the user is satisfied with the output.

134

135 2.2. Feature extraction

136 After the image analysis, the dataset is extracted from the image using the function **ExtractData**.
137 This function extracts the coordinates of all the points lying on boundary, all the points lying
138 inside the boundary and the relevant geometric data generated from GrabImage function (from
139 task (iii)). The ExtractData function utilises in-built Mathematica functions to perform these
140 tasks, for e.g., FindShortestTour function is used for ordering boundary points. These data are
141 passed on collectively as input to further functions to compute the shape and size of particles.
142 Additionally, two geometric features – diameter of inscribed circle and circumscribed circle - are
143 computed for calculation of textural parameters (listed in section 2.3). They are only stored
144 internally and are fed into functions that require them. The radius and the centre of the largest
145 inscribed circle of each particle is computed by the function **InscribedCircle**. Here the minimum
146 distance from any point inside the particle boundary to the particle boundary is maximised using
147 discrete optimisation with multiple starting points. Similarly, **CircumscribedCircle** function
148 computes the smallest circumscribing circle over the particle boundary by minimising the
149 maximum distance from any point inside the particle boundary to the particle boundary.

150 2.3. Computation of textural parameters

151 Measurements in this paper are focused on a 2-dimensional representation of the particle
152 boundary. In case of loose sediments, projection of particles along the long and intermediate axis
153 is taken, whereas, a 2D section of sediments cutting across consolidated sample is available from
154 a thin section. A large number of parameters have been proposed to quantify particle shape
155 (Barrett, 1980; Blott and Pye, 2008 and references therein). It is difficult to select one parameter
156 out of the many available, that allows for consistent, reliable and accurate distinction between
157 particles of different shapes. As a result, the relative merits of different shape parameters have
158 been extensively reviewed along with the many practical studies making comparisons (Al-
159 Rousan et al., 2007; Barrett, 1980; Blott and Pye, 2008; Cox and Budhu, 2008; Illenberger,
160 1991). In light of their application to 2-D image data, the following parameters are discussed and
161 implemented: roundness, circularity, irregularity, angularity, fractal dimension, Fourier
162 descriptors and a number of other simpler dimensionless parameters such as aspect ratio,
163 rectangularity, convexity, modratio, compactness and solidity. Additionally, a variety of size
164 parameters are implemented. The implementation details and description of parameters are
165 described below:

166 2.3.1. Roundness

167 The most widely accepted definition of roundness (Wadell, 1932) is that it is the average
168 roundness of the corners of a particle in a 2-D sectional plane. Let r be the radius of curvature of
169 the boundary and let r_{max} be the radius of the largest inscribed circle to the particle boundary.
170 Corners are those parts of the particle boundary where $r < r_{max}$. Particle roundness (R) is
171 defined as:

$$R = \frac{1}{n r_{max}} \sum_{i=1}^n r_i$$

172 where r_i is the radius of curvature of individual corner and n is the total number of corners.
 173 Roundness can now be determined in a time efficient and objective manner using computational
 174 image analysis techniques (Roussillon et al., 2009; Tunwal et al., 2018).

175 The **Roundness** function first calculates the radius of curvature at each point on the boundary. It
 176 makes use of the function **CircumRadius**, which determines the radius of the circle
 177 circumscribing three points: 1) i th pixel at which radius of curvature is to be determined, 2)
 178 $(i+n)$ th pixel and 3) $(i-n)$ th pixel (see Fig. 4a). The value of n is normalised on the basis of total
 179 number of boundary points in the particle. In Figure 4, point A, B and C represents the $(i - n)$ th,
 180 i th and $(i + n)$ th pixel respectively. Points with a radius of curvature greater than radius of the
 181 largest inscribed circle of the particle (from **InscribedCircle** function) are omitted (see Fig. 4b).
 182 The mean of the radius of curvature of the remaining points divided by radius of the largest
 183 inscribed circle is the roundness.

184

185 2.3.2. Circularity

186 Circularity is a measure of how closely a particle boundary approximates to a circle. Typical
 187 circularity parameters (Cox, 1927; Janoo, 1998; Pentland, 1927; Riley, 1941; Wadell, 1933;
 188 Wadell, 1935) were applied to 23 gravel particles in a comparison study (Blott and Pye, 2008).
 189 They found that the methods of Wadell (1935) and Riley (1941) provided optimal results. Due to
 190 its simplicity and similarity to Wadell (1935), Riley (1941) was considered to be the best
 191 parameter and is implemented in IPSAT. It is given by:

$$C = \sqrt{(D_I/D_c)}$$

192 where C is the circularity, D_I is the diameter of largest inscribed circle and D_c is the diameter of
 193 smallest circumscribing circle (see Fig. 5). The **CircularityFunction** takes radius of the largest
 194 inscribed circle of the particle from `InscribedCircle` and the radius of the smallest circumscribing
 195 circle of the particle from `CircumscribedCircle` to compute circularity.

196 2.3.3. Irregularity

197 Irregularity has been recently suggested as a parameter to describe particle shape (Blott and Pye,
 198 2008). It is defined as a way to measure the indentations and projections of a particle boundary
 199 with respect to the best fit ellipse (Tunwal et al., 2018). It is given by:

$$I = A_U/A_E$$

200 Where I is the irregularity, A_U is the non-overlapping area and A_E is the area of ellipse (see Fig.
 201 6). The value for irregularity varies in the range 0 to 1. Particle with smooth boundary exhibits
 202 lower value for irregularity as compared to a particle with irregular boundary. The **Irregularity**
 203 function generates two matrices for each particle: the first represents points belonging to the
 204 particle and the second consists of points inside the best-fit ellipse of the particle. Thus, addition
 205 of the matrices identifies the non-overlapping region used for calculating irregularity.

206 2.3.4. Angularity

207 Angularity is usually considered the opposite of roundness, however it is formally defined as a
 208 shape parameter based on acuteness of angle of corners, number of corners and projection of
 209 corners from the centre of particle (Lees, 1964). To measure angularity, the **Angularity** function
 210 converts the particle boundary into a n sided polygon by sampling n points at regular interval
 211 along the particle boundary points (Rao et al., 2002). The internal angle at each vertex is

212 computed, which is represented by α_1 to α_n . The difference between the pair of consecutive
 213 angles ($\alpha_1-\alpha_2$, $\alpha_2-\alpha_3$ to $\alpha_n-\alpha_1$) of the polygon is calculated for all vertices (see Fig. 7). The average
 214 of the five largest differences of angles is the angularity (Tunwal et al., 2018). The number of
 215 sides of regular polygon that represents the particle boundary and the number of highest
 216 differences of consecutive angles can be varied by user.

217 2.3.5. Fractal dimension

218 Benoit Mandelbrot is credited with discovering the field of Fractal geometry in mathematics to
 219 characterise irregular shapes and quantify their roughness (Mandelbrot, 1982). Using fractal
 220 dimension as a measure of roughness in granular materials is already established (Andrle, 1992;
 221 Cox and Budhu, 2008; Hyslip and Vallejo, 1997; Tunwal et al., 2018).

222 The **FractalDivider** function is implemented in IPSAT using the divider method. This method
 223 essentially measures the length of the boundary using different measuring sticks and uses the
 224 relationship between the two to estimate the fractal dimension (see Fig. 8a). If the length of the
 225 boundary of a shape is measured to be $P(\lambda)$, using measure of length λ then

$$P(\lambda) = n\lambda^{1-D}$$

226 where D is the fractal dimension and n is a constant of proportionality, which depends on the
 227 actual length of the boundary being analysed. Lower values of λ result in more accurate and
 228 increased estimates of boundary length $P(\lambda)$. Taking logarithms:

229

$$\log P(\lambda) = \log n + (1 - D) \log \lambda$$

230 thus D may be readily estimated by finding the best fit straight line to a set of data of
231 $(\log \lambda, \log P(\lambda))$ (see Fig. 8b). The unit divider length λ in IPSAT depend on the size of each
232 individual particle (normalised based on the axes of the best fit ellipse).

233 2.3.6. Fourier method

234 Half a century ago, Fourier analysis was introduced as an accurate way to characterise sediment
235 particle shape (Schwarcz and Shane, 1969; Ehrlich and Weinberg, 1970). Fourier analysis is
236 based on the fact that any periodic function can be represented by a series of sine and cosine
237 terms. Fourier analysis is applied in shape characterisation by unrolling the particle boundary and
238 treating it as a periodic wave function and using the centroid of the particle as the origin. The
239 particle boundary can be reconstructed to a high degree of accuracy by using a suitable number
240 of terms. In spite of being robust, Fourier analysis in this context is not ideal due to the re-entrant
241 angle problem. Re-entrants are due to jagged or crenellate edge morphology in irregular shaped
242 particles (Orford and Whalley, 1983) and leads to re-entrant angle or multi-valued function
243 problem (Bowman et al., 2001; Thomas et al., 1995). To overcome the shortcoming of re-entrant
244 angle, Fourier descriptors are used (Thomas et al., 1995).

245 In this technique, the particle boundary is first sampled at regular intervals. Each boundary point
246 is represented in the complex plane by:

247

$$z_m = x_m + i y_m$$

248

249 where (x_m, y_m) are the coordinates, m goes from 0 to $(N - 1)$ and N is the total number of
 250 sampled points. The discrete Fourier transform is applied to the list of boundary points to obtain
 251 the list of descriptors as follows:

252

$$Z_k = \frac{1}{N} \sum_{m=0}^{N-1} z_m e^{-i \frac{2\pi mk}{N}} = \frac{1}{N} \sum_{m=0}^{N-1} z_m \left(\cos \frac{2\pi mk}{N} - i \sin \frac{2\pi mk}{N} \right)$$

253

254 The Fourier descriptors are $Z_k = a_k + ib_k$ where k takes the values 0 to $N - 1$.

255 Applying the inverse Fourier transform to the descriptors retrieves estimates of the boundary
 256 points of a particle and thus can be used to reconstruct the original shape of the particle. Often
 257 only a subset of the full set of Fourier descriptors are utilised for a particle. As the number of
 258 Fourier descriptors used to describe a shape increases, the boundary retrieved by the inverse
 259 transform becomes more accurate (see Fig. 9). Descriptors with low values of k tend to describe
 260 the major features of a particle whereas those with high values of k describe the finer
 261 morphological details.

262 Fourier descriptors are computed using the **FourierDescriptor** function. In this function, the
 263 boundary is sampled at regular interval to take a total of n points for each particle, where n can
 264 be set by user. The centre of the particle boundary is shifted to the origin to compute the n
 265 number of Fourier descriptors. The output to a file type of user's choice can be exported using
 266 **FourierOutput** function.

267 2.3.7. Other parameters

268 Shape parameters, which were traditionally not taken into account from a sedimentological point
269 of view but can prove useful in discriminating different types of sedimentary particles, are also
270 included in IPSAT. Cox and Budhu (2008) studied many simple parameters and identified key
271 parameters to discriminate amongst sedimentary particles (see Table 1). These parameters are
272 calculated directly using basic geometric features extracted earlier (see section 2.2). They can be
273 viewed and exported along with other results using ResultTable function described in section
274 2.4.

275 2.3.8 Particle Size

276 In this paper, the size of sand particles is measured using image analysis techniques on a
277 microphotograph. However, the methodology presented here can be extended to images of
278 particles from other size fractions. **SizeData** function is written to compute the actual size of
279 particle regions by parameters listed in Table 2. The user is required to specify the actual width
280 of the input image so that IPSAT can convert pixel units to standard physical units (i.e. microns
281 or millimetres). Thus it has three arguments: the output from GrabImage, CircumscribedCircle
282 and the actual width.

283 Due to slicing of grains in thin section, the measured size of a particle from a thin section
284 microphotograph is usually less than the size measured from the projection on a loose grain
285 (Burger and Skala, 1976). There are multiple approaches in the field stereology to transform a 2-
286 D particle size distribution to a 3-D size distribution (Mouton, 2011; Russ and Dehoff, 2000).
287 Some authors have recommended using a simple multiplication factor for the size transformation
288 (for example, Harrell and Eriksson, 1979; Kong et al., 2005), however, others have
289 recommended using a size distribution transformation algorithm (Heilbronner and Barrett, 2014;

290 Higgins, 2000; Peterson, 1996). In this paper, one such , which assumes that the probability of
291 slicing a particle is dependent on its size and distance from centre is implemented (Heilbronner
292 and Barrett, 2014; Underwood, 1970).

293 The **SizeTransform** function is available to convert a 2-D size distribution to a 3-D size
294 distribution. This function takes data from **SizeData** as input along with class distribution width
295 and the numeral code for the type of size parameter to be used. The algorithm implemented in
296 IPSAT follows the method described in Heilbronner and Barrett (2014) for STRIPSTAR
297 program.

298 2.4. Results

299 Results obtained for all particles in a sample can be summarised in tabular form and exported to
300 an excel file. Users can specify the parameters they wish to include in the output. The function
301 **ResultTable**[*exdata_*, *parameters_*, *others_*, *sizedata_*] is written for this purpose. The argument
302 *parameters_* specifies the list of parameters that are required by the user. This provides
303 flexibility and saves execution time. The third argument *others_* may be either *True* or *False* and
304 indicates whether or not to include in the output the other parameters in the result table. The
305 fourth argument *sizedata_* takes in the output from **SizeData**, if size is required. These other
306 parameters include simple geometric data such as aspect ratio, rectangularity, convexity,
307 modratio, compactness and solidity (see Table 1).

308 Finally, a data visualisation function called **GrainMapping** is present to display regions of
309 particle using varying colour scheme based on output of a chosen shape or size parameter (see
310 Fig. 10). This feature has been used in other image analysis tools (e.g. Heilbronner and Barrett,
311 2014) and is presented here for completeness.

312 3. Example Analysis

313 One sample each of unconsolidated (loose sediment) and consolidated (rock thin section) is
314 analysed to demonstrate the usage of this software package. A total of 60 particles were analysed
315 for both examples. Details of the samples and their image preparation methodology are discussed
316 below.

317 3.1. Loose sediment

318 A loose sediment sample from Ballycotton beach, County Cork, Ireland was collected for
319 particle shape analysis. The sample is dry sieved to separate the different size fractions. For
320 example analysis, the 250 to 500 Microns size fraction is used. The sand grains are carefully
321 settled on the microscope stage parallel to their longest and intermediate axis. Using a paint
322 brush, these particles are set up such that they do not touch each other and remain within the
323 field of view of the microscope. For each field of view, 5-7 particles were imaged (see Fig. 2a).
324 The images were captured at 140X for 1640*2186 microns field of view at 1200*1600 Pixel
325 resolution. The following settings were used for the microscope for transmitted light from
326 beneath the stage: exposure 61.4 ms; saturation: 1.3; gain: 1.0X; gamma 1.29.

327 3.2. Rock thin section

328 A sandstone sample from Dingle Basin, South-West Ireland was collected for thin section
329 analysis. The sample collected is from the Eask Sandstone Formation of the Dingle group and is
330 relatively undeformed. The sediment particles in the sample were deposited in a fluvial type of
331 depositional environment during the Lower Devonian (Allen and Crowley, 1983). The sample
332 shows poorly sorted quartz grains surrounded by a clay matrix (Fig. 3a).

333 Thin section images of each sample in cross-polarised light were used for tracing out particle
334 boundaries. Using more than one image of the same field of view at different stage orientations
335 in cross-polarised light may increase clarity for tracing particle boundaries. An Intuos Pro
336 Graphics Tablet was used to digitally trace the boundaries in CorelDRAW, which is a vector
337 graphics editing software. Digital tracing of particle boundaries allows the flexibility of zooming
338 in and out on the field of view and browse through microphotographs at different stage
339 orientations while tracing. Each particle boundary is traced carefully so that they form a closed
340 loop otherwise they are not detected as a separate region during the image processing step. It is
341 important to ensure that the particle boundaries do not touch each other (Fig. 3b). The particle
342 boundaries can be alternately traced physically on a tracing sheet and digitised for analysis (refer
343 to Mulchrone et al. (2013) for details). The traced image is 1.86 Mb in size (1600*1200 pixels).
344 The physical size of the thin section image is 1640*2186 Microns determined using Leica
345 Microscope software.

346 4. Results and Discussion

347 The result of particle shape analysis for the loose sediment sample is presented in the form of
348 histogram (Fig. 11). Roundness, angularity, irregularity and fractal dimension data display a
349 normal distribution. Circularity data for the population show a negative skew, whereas, there is
350 positive skewness in the aspect ratio data distribution. The mean and standard deviation of:
351 roundness is 0.61 and 0.04; angularity is 54.04 and 10.93; irregularity is 0.14 and 0.05; and
352 fractal dimension is 1.02 and 0.01 respectively. The median of circularity and aspect ratio data is
353 0.82 and 1.32 respectively.

354 Figure 12 shows the population distribution of shape parameters from the sandstone thin section
355 sample. The datasets of roundness, circularity, irregularity and angularity exhibit normal

356 distributions, whereas, fractal dimension and aspect ratio show positively skewed distributions.
357 The mean and standard deviation of: roundness is 0.60 and 0.04; circularity is 0.76 and 0.06;
358 irregularity is 0.17 and 0.05; and angularity is 53.92 and 10.94. The median of fractal dimension
359 and aspect ratio is 1.03 and 1.51 respectively.

360 The image analysis package –IPSAT presented in this paper can be used to measure a range of
361 shape and size parameters. More than one shape parameter can be used to better characterise a
362 particle shape (Blott and Pye, 2008). The shape parameters implemented here were tested on
363 regular geometric shapes (Blott and Pye, 2008) and were found to perform well. A previous
364 study by the authors (Tunwal et al., 2018) found angularity and fractal dimension to be the most
365 important parameters for classifying sediment samples in their textural maturity grouping.
366 However, presence of a comprehensive list of shape parameters in IPSAT offers a choice to users
367 from diverse research objectives. It is to be noted that the term angularity, roundness and
368 circularity are defined differently in various software tools. For e.g., roundness in ImageJ
369 (Schneider et al., 2012) refers to the ratio $4Area/\pi(MajorAxis)^2$, whereas, roundness in
370 IPSAT is based on calculation of radius of curvature at each boundary point (Roussillon et al.,
371 2009). Fourier descriptors, function available in IPSAT, exports fourier descriptor data in raw
372 form. This is to facilitate users the flexibility to choose their preferred way of further analysis
373 (for e.g., Bowman et al., 2001; Charpentier et al., 2013; Suzuki et al., 2015; Thomas et al., 1995;
374 Haines and Mazzullo, 1988; Sarocchi et al., 2011).

375 IPSAT offers a variety of size parameters for analysis. Different measures of size give different
376 particle size distributions for the same population of particles (Heilbronner and Barrett, 2014).
377 Therefore, a suite of size parameters implemented here gives the user the freedom to pick the
378 parameters of choice. For thin section images, 2-Dimensional particle size distribution should be

379 transformed into 3-Dimensional size distribution for analysis. Apart from the shape and size
380 parameters presented in IPSAT, some additional information regarding the particles can be
381 further obtained implicitly from the results. For example, area and perimeter of particles can be
382 calculated from the size measures S_d and S_p . Such information can be extracted, if required, by
383 the user.

384 The manual particle boundary tracing for thin section analysis can be regarded by some as a
385 tedious exercise. However, in the light of unavailability of an automated particle boundary
386 segmentation algorithm that can be used for any type of thin section image, manual particle
387 boundary tracing provides the best alternative at present. High quality shape and size information
388 can be easily obtained once the boundary is traced. Furthermore, the whole methodology is
389 relatively cheap to perform. If new analysis techniques emerge which can process messy natural
390 data, the analysis software presented here will be fully compatible and the process can be fully
391 automated.

392 The shape parameters calculated using particle boundary data in this package is independent of
393 size. However, a particle of a very small pixel size is prone to be affected by its size for shape
394 calculation (Kröner and Doménech Carbó, 2013). Regular geometric and irregular shape with
395 increasing pixel count were used to test this package to check variation of parameter values with
396 varying pixel count for a fixed shape. It was found it is not affected by size (S_c) above 85 pixels.
397 Thus, size limit for textural analysis of sediment is based on the image acquisition tool.
398 Furthermore, a higher pixel resolution is recommended for good results.

399 The contribution presented here will help in filling the gap for a specialised texture analysis
400 toolbox in the domain of sedimentology. The use of the software package introduced here has
401 been demonstrated by examples with sand sized particles. However, it can be used for particles

402 of any size. Therefore, the image analysis package can be of use to variety of users for diverse
403 shape analysis objectives.

404 5. Conclusion

405 In this paper, IPSAT – Image based Particle Shape Analysis Toolbox is presented for
406 determination of textural elements of sedimentary particles. A suite of 12 shape parameters and 6
407 size parameters are implemented in IPSAT. Usage of the presented toolbox has been
408 demonstrated using photomicrographs from a sandstone thin section and a loose sediment
409 sample. Manual tracing of particles of thin section particle boundaries is recommended, whereas,
410 a fully automated approach is available for loose sediment analysis.

411 The software along with the methodology proposed in this paper, has the potential for allowing
412 access to quantitative data for textural elements of siliciclastic particles. Thus, it has the potential
413 to provide important information for a wide range of sedimentary studies. Future work in the
414 direction of quantitative textural analysis of sedimentary particles include development of a
415 statistical approach aimed at synthesis and analysis of distributions of sediment particle shape
416 population data.

417

418 6. Acknowledgement

419 The authors are thankful to the Chief Editor and the three anonymous reviewers for their
420 suggestions which has substantially improved the manuscript. This project was funded by the
421 Irish Shelf Petroleum Studies Group (ISPSG) of the Irish Petroleum Infrastructure Programme
422 (PIP).

423 7. Computer Code Availability

424 The Image based Particle Shape Analysis Toolbox (IPSAT) is developed as a Mathematica
425 package (26 Kb). The IPSAT code is written on Wolfram language which requires Mathematica
426 environment to function. The IPSAT package is released under the GPL3 license. The IPSAT
427 code along with a detailed user manual can be downloaded from
428 <https://github.com/tunwalm/IPSAT>. The developer can be contacted reached by the following:

429 Email: mohit.tunwal@ucc.ie

430 Telephone: +353-21-490-4580

431 Address: School of BEES, University College Cork, Distillery Fields, North Mall, Cork, T23
432 TK30, Ireland

433

434 8. References

435

436 **Al-Rousan, T., Masad, E., Tutumluer, E. and Pan, T.** (2007) Evaluation of image analysis techniques for
437 quantifying aggregate shape characteristics. *Construction and Building Materials*, **21**, 978-990.

438 **Allen, J.R.L. and Crowley, S.F.** (1983) Lower Old Red Sandstone fluvial dispersal systems in the British
439 Isles. *Transactions of the Royal Society of Edinburgh: Earth Sciences*, **74**, 61-68.

440 **Andrle, R.** (1992) Estimating fractal dimension with the divider method in geomorphology.
441 *Geomorphology*, **5**, 131-141.

442 **Barrett, P.J.** (1980) The shape of rock particles, a critical review. *Sedimentology*, **27**, 291-303.

443 **Blatt, H.** (1992) *Sedimentary Petrology*. W. H. Freeman and Company, New York, 514 pp.

- 444 **Blatt, H., Middleton, G. and Murray, R.** (1972) Origin of Sedimentary Rocks. Prentice-Hall Inc., Upper
445 Saddle, NJ, 634 pp.
- 446 **Blott, S.J. and Pye, K.** (2008) Particle shape: a review and new methods of characterization and
447 classification. *Sedimentology*, **55**, 31-63.
- 448 **Bowman, E.T., Soga, K. and Drummond, W.** (2001) Particle shape characterisation using Fourier
449 descriptor analysis. *Géotechnique*, **51**, 545-554.
- 450 **Burger, H. and Skala, W.** (1976) Comparison of sieve and thin-section technique by a Monte-Carlo
451 model. *Computers & Geosciences*, **2**, 123-139.
- 452 **Calderon De Anda, J., Wang, X.Z. and Roberts, K.J.** (2005) Multi-scale segmentation image analysis for
453 the in-process monitoring of particle shape with batch crystallisers. *Chemical Engineering Science*, **60**,
454 1053-1065.
- 455 **Campañá, I., Benito-Calvo, A., Pérez-González, A., Bermúdez de Castro, J.M. and Carbonell, E.** (2016)
456 Assessing automated image analysis of sand grain shape to identify sedimentary facies, Gran Dolina
457 archaeological site (Burgos, Spain). *Sedimentary Geology*, **346**, 72-83.
- 458 **Charpentier, I., Sarocchi, D. and Rodriguez Sedano, L.A.** (2013) Particle shape analysis of volcanic clast
459 samples with the Matlab tool MORPHEO. *Computers & Geosciences*, **51**, 172-181.
- 460 **Cox, E.P.** (1927) A Method of Assigning Numerical and Percentage Values to the Degree of Roundness of
461 Sand Grains. *Journal of Paleontology*, **1**, 179-183.
- 462 **Cox, M.R. and Budhu, M.** (2008) A practical approach to grain shape quantification. *Engineering*
463 *Geology*, **96**, 1-16.
- 464 **Eamer, J.B.R., Shugar, D.H., Walker, I.J., Lian, O.B. and Neudorf, C.M.** (2017) Distinguishing depositional
465 setting for sandy deposits in coastal landscapes using grain shape. *Journal of Sedimentary Research*, **87**,
466 1-11.

- 467 **Ehrlich, R. and Weinberg, B.** (1970) An exact method for characterization of grain shape. *Journal of*
468 *Sedimentary Research*, **40**, 205-212.
- 469 **Gorsevski, P.V., Onasch, C.M., Farver, J.R. and Ye, X.** (2012) Detecting grain boundaries in deformed
470 rocks using a cellular automata approach. *Computers & Geosciences*, **42**, 136-142.
- 471 **Haines, J. and Mazzullo, J.** (1988) The original shapes of quartz silt grains: A test of the validity of the use
472 of quartz grain shape analysis to determine the sources of terrigenous silt in marine sedimentary
473 deposits. *Marine Geology*, **78**, 227-240.
- 474 **Harrell, J.A. and Eriksson, K.A.** (1979) Empirical conversion equations for thin-section and sieve derived
475 size distribution parameters. *Journal of Sedimentary Research*, **49**, 273-280.
- 476 **Heilbronner, R. and Barrett, S.** (2014) *Image analysis in earth sciences: microstructures and textures of*
477 *earth materials*. Springer, Heidelberg, 513 pp.
- 478 **Higgins, M.D.** (2000) Measurement of crystal size distributions. *American Mineralogist*, **85**, 1105-1116.
- 479 **Higgins, M.D.** (2006) *Quantitative textural measurements in igneous and metamorphic petrology*.
480 Cambridge University Press, Cambridge, 265 pp.
- 481 **Hyslip, J.P. and Vallejo, L.E.** (1997) Fractal analysis of the roughness and size distribution of granular
482 materials. *Engineering Geology*, **48**, 231-244.
- 483 **Illenberger, W.K.** (1991) Pebble shape (and size!). *Journal of Sedimentary Research*, **61**, 756-767.
- 484 **Janoo, V.** 1998. Quantification of shape, angularity, and surface texture of base course materials, Cold
485 Regions Research and Engineering Lab Hanover NH.
- 486 **Kong, M., Bhattacharya, R.N., James, C. and Basu, A.** (2005) A statistical approach to estimate the 3D
487 size distribution of spheres from 2D size distributions. *GSA Bulletin*, **117**, 244-249.
- 488 **Kröner, S. and Doménech Carbó, M.T.** (2013) Determination of minimum pixel resolution for shape
489 analysis: Proposal of a new data validation method for computerized images. *Powder Technology*, **245**,
490 297-313.

- 491 **Krumbein, W.C.** (1941) Measurement and geological significance of shape and roundness of
492 sedimentary particles. *Journal of Sedimentary Research*, **11**, 64-72.
- 493 **Lees, G.** (1964) A NEW METHOD FOR DETERMINING THE ANGULARITY OF PARTICLES. *Sedimentology*, **3**,
494 2-21.
- 495 **Li, Y., Onasch, C.M. and Guo, Y.** (2008) GIS-based detection of grain boundaries. *Journal of Structural*
496 *Geology*, **30**, 431-443.
- 497 **Lira, C. and Pina, P.** (2009) Automated grain shape measurements applied to beach sands. *Journal of*
498 *Coastal Research*, 1527-1531.
- 499 **Mandelbrot, B.B.** (1982) *The Fractal Geometry of Nature*. W. H. Freeman and Company, New York, NY,
500 468 pp.
- 501 **Mingireanov Filho, I., Vallin Spina, T., Xavier Falcão, A. and Campana Vidal, A.** (2013) Segmentation of
502 sandstone thin section images with separation of touching grains using optimum path forest operators.
503 *Computers & Geosciences*, **57**, 146-157.
- 504 **Moreno Chávez, G., Castillo Rivera, F., Sarocchi, D., Borselli, L. and Rodríguez-Sedano, L.** (2018)
505 *FabricS: A user-friendly, complete and robust software for particle shape-fabric analysis. Computers &*
506 *Geosciences*, **115**, 20-30.
- 507 **Moreno Chávez, G., Sarocchi, D., Arce Santana, E. and Borselli, L.** (2015) Optical granulometric analysis
508 of sedimentary deposits by color segmentation-based software: OPTGRAN-CS. *Computers &*
509 *Geosciences*, **85**, 248-257.
- 510 **Mouton, P.R.** (2011) *Unbiased stereology: a concise guide*. JHU Press, Baltimore, Maryland, 200 pp.
- 511 **Mulchrone, K.F., McCarthy, D.J. and Meere, P.A.** (2013) Mathematica code for image analysis, semi-
512 automatic parameter extraction and strain analysis. *Computers & Geosciences*, **61**, 64-70.
- 513 **Orford, J.D. and Whalley, W.B.** (1983) The use of the fractal dimension to quantify the morphology of
514 irregular-shaped particles. *Sedimentology*, **30**, 655-668.

- 515 **Pentland, A.** (1927) A method of measuring the angularity of sands. Proceedings and Transactions of the
516 Royal Society of Canada, **21**, xciii.
- 517 **Peterson, T.D.** (1996) A refined technique for measuring crystal size distributions in thin section.
518 Contributions to Mineralogy and Petrology, **124**, 395-405.
- 519 **Pettijohn, F.J.** (1957) Sedimentary Rocks. Harper & Brothers, New York, 718 pp.
- 520 **Powers, M.C.** (1953) A new roundness scale for sedimentary particles. Journal of Sedimentary Research,
521 **23**, 117-119.
- 522 **Rao, C., Tutumluer, E. and Kim, I.T.** (2002) Quantification of Coarse Aggregate Angularity Based on
523 Image Analysis. Transportation Research Record: Journal of the Transportation Research Board, **1787**,
524 117-124.
- 525 **Riley, N.A.** (1941) Projection sphericity. Journal of Sedimentary Research, **11**, 94-97.
- 526 **Roduit, N.** (2007) JMicroVision: un logiciel d'analyse d'images pétrographiques polyvalent. Ph.D.
527 Dissertation, University of Geneva, Geneva, Switzerland, 112pp.
- 528 **Roussillon, T., Piégay, H., Sivignon, I., Tougne, L. and Lavigne, F.** (2009) Automatic computation of
529 pebble roundness using digital imagery and discrete geometry. Computers & Geosciences, **35**, 1992-
530 2000.
- 531 **Roy Choudhury, K., Meere, P.A. and Mulchrone, K.F.** (2006) Automated grain boundary detection by
532 CASRG. Journal of Structural Geology, **28**, 363-375.
- 533 **Russ, J.C. and Dehoff, R.T.** (2000) *Practical stereology*. Plenum Publishers, New York, 381 pp.
- 534 **Sarocchi, D., Sulpizio, R., Macías, J.L. and Saucedo, R.** (2011) The 17 July 1999 block-and-ash flow (BAF)
535 at Colima Volcano: New insights on volcanic granular flows from textural analysis. *Journal of Volcanology
536 and Geothermal Research*, **204**, 40-56.
- 537 **Schneider, C.A., Rasband, W.S. and Eliceiri, K.W.** (2012) NIH Image to ImageJ: 25 years of image
538 analysis. Nature Methods, **9**, 671-675.

- 539 **SCHWARCZ, H.P. and SHANE, K.C.** (1969) MEASUREMENT OF PARTICLE SHAPE BY FOURIER ANALYSIS.
540 *Sedimentology*, **13**, 213-231.
- 541 **Sochan, A., Zieliński, P. and Bieganski, A.** (2015) Selection of shape parameters that differentiate
542 sand grains, based on the automatic analysis of two-dimensional images. *Sedimentary Geology*, **327**, 14-
543 20.
- 544 **Suzuki, K., Fujiwara, H. and Ohta, T.** (2015) The evaluation of macroscopic and microscopic textures of
545 sand grains using elliptic Fourier and principal component analysis: Implications for the discrimination of
546 sedimentary environments. *Sedimentology*, **62**, 1184-1197.
- 547 **Takashimizu, Y. and Iiyoshi, M.** (2016) New parameter of roundness R: circularity corrected by aspect
548 ratio. *Progress in Earth and Planetary Science*, **3**, 1-16.
- 549 **Tao, J., Zhang, C., Qu, J., Yu, S. and Zhu, R.** (2018) A de-flat roundness method for particle shape
550 quantitative characterization. *Arabian Journal of Geosciences*, **11**, 414.
- 551 **Thomas, M.C., Wiltshire, R.J. and Williams, A.T.** (1995) The use of Fourier descriptors in the
552 classification of particle shape. *Sedimentology*, **42**, 635-645.
- 553 **Trott, M.** (2013) *The Mathematica guidebook for programming*. Springer, New York, 1027 pp.
- 554 **Tunwal, M., Mulchrone, K.F. and Meere, P.A.** (2018) Quantitative characterization of grain shape:
555 Implications for textural maturity analysis and discrimination between depositional environments.
556 *Sedimentology*, **65**, 1761-1776.
- 557 **Underwood, E.E.** (1970) *Quantitative Stereology*. Addison-Wesley Pub. Co., Reading, Mass., 274 pp.
- 558 **Wadell, H.** (1932) Volume, Shape, and Roundness of Rock Particles. *The Journal of Geology*, **40**, 443-451.
- 559 **Wadell, H.** (1933) Sphericity and roundness of rock particles. *The Journal of Geology*, **41**, 310-331.
- 560 **Wadell, H.** (1935) Volume, Shape, and Roundness of Quartz Particles. *The Journal of Geology*, **43**, 250-
561 280.

562 **Wellin, P.R., Gaylord, R.J. and Kamin, S.N.** (2005) *An introduction to programming with Mathematica*[®].
563 Cambridge University Press, Cambridge, UK, 570 pp.

564

565

566

567

568

569

570

571

572

573 **Figure Captions**

574 *Figure 1: Flowchart showing functionality of IPSAT program.*

575 *Figure 2: Image analysis routine for loose sediment analysis. (a) Shows microphotograph of*
576 *loose sand sample collected from Ballycotton, County Cork, Ireland. (b) Particle boundary of the*
577 *sediment grains from the loose sediment sample is automatically generated using IPSAT (c)*
578 *image analysis of particle boundary shows region in randomly assigned colours identified as*
579 *individual particles.*

580 *Figure 3: Image analysis routine for a compacted sample (a) Shows thin section*
581 *microphotograph of sandstone sample collected from Dingle, County Kerry, Ireland. (b) Particle*

582 boundary of the clasts from thin section is manually traced using a graphics tablet (c) image
 583 analysis of traced particle boundary shows region in randomly assigned colours identified as
 584 individual particles.

585 Figure 4: Roundness measurement of a particle boundary. (a) Calculation of radius of curvature
 586 at the i th pixel point B is the radius of circle that passes through the points A, B and C . The
 587 points A and C are the $(i + n)^{th}$ pixel and $(i - n)^{th}$ pixel where n is normalised on the basis
 588 total number of boundary points. (b) The particle boundary points with radius of curvature lower
 589 than the radius of largest inscribing circle represents the corner region and are thus accepted
 590 for roundness calculation.

591 Figure 5: Circularity of particle measured by square root over the ratio of diameter of the
 592 largest inscribed circle (D_i) divided by the diameter of the smallest circumscribed circle (D_c).

593 Figure 6: Measurement of particle irregularity. (a) Particle boundary to be analysed. (b) Best fit
 594 ellipse for the particle boundary to be analysed. (c) Overlap of best fit ellipse over the particle
 595 boundary. Irregularity is measured as a ratio of area not common between ellipse and particle
 596 boundary divided by the area of ellipse.

597 Figure 7: Angularity measurement of a particle by modified Rao et al. (2002). Particle boundary
 598 is represented by n sided polygon. Internal angles $\alpha_1, \alpha_2, \alpha_3$ till α_n for the polygon is measured.
 599 Differences within the successive internal angles is measured and the five largest differences of
 600 internal angles are averaged to calculate angularity.

601 Figure 8: Fractal dimension calculation for a particle using the divider method. (a) Particle
 602 boundary perimeter $P(\lambda)$ measured by increasing unit length λ . The value of m is 13.28 pixel

603 dimension based on the size of the particle. (b) $\text{Log } P(\lambda)$ versus $\text{Log } \lambda$ showing the fractal
 604 dimension (D) calculation.

605 Figure 9: Reconstructed particle boundary with the number of Fourier descriptors used from
 606 $k=1$ to 15. Shows the increasing accuracy of the particle boundary with the number of
 607 descriptors used.

608 Figure 10: Grain-map of thin section sample for angularity parameter. The colour varies from
 609 light green for highest roundness to dark blue for highest angularity value.

610 Figure 11: Results from photomicrograph analysis of loose sediment sample represented by
 611 histogram for: (a) roundness; (b) circularity; (c) irregularity; (d) angularity; (e) fractal
 612 dimension; and (f) aspect ratio data

613 Figure 12: Results from thin section photomicrograph analysis of sandstone sample represented
 614 by histogram for: (a) roundness; (b) circularity; (c) irregularity; (d) angularity; (e) fractal
 615 dimension; and (f) aspect ratio data

616

617 Tables

618

619

620

Shape Parameter	Formula	Description
Aspect Ratio	$L_{\text{major}}/L_{\text{minor}}$	Length of major axis (L_{major}) by length of minor axis

		(L_{minor})
Compactness	$\sqrt{4A/\pi}/L_{major}$	Diameter of circle of equivalent area (A) to particle by length of major axis (L_{major})
ModRatio	$2R_I/\text{Feret}$	Diameter of largest inscribed circle (R_I) divided by Feret diameter
Solidity	A/A_{convex}	Area (A) by convex area (A_{convex})
Convexity	P_{convex}/P	Convex perimeter (P_{convex}) by perimeter of particle (P)
Rectangularity	A/A_{BR}	Area of particle (A) by area of bounding rectangle (A_{BR})

621

622

Table 1: Table of simple geometrical parameters used in the study.

623

624

625

626

627

628

Size parameter	Formula	Description
S_c	D_c	Diameter of smallest circumscribing circle over a particle boundary

S_p	P/π	Perimeter of particle boundary (P) divided by π
S_d	$\sqrt{4A/\pi}$	Diameter of equivalent disk area of the particle. Here A is the area of the particle.
S_a	L_{major}	Long axis of the best fit ellipse (L_{major})
S_b	L_{minor}	Short axis of the best fit ellipse (L_{minor})
S_m	$\frac{2 \sum_{i=1}^n (d_i)}{n}$	Twice of the mean distance between centre and particle boundary. Here d_i is the distance between centroid of the particle to its i th boundary point and n is the number of boundary points.

629

630

Table 2: List of size parameters implemented in IPSAT.

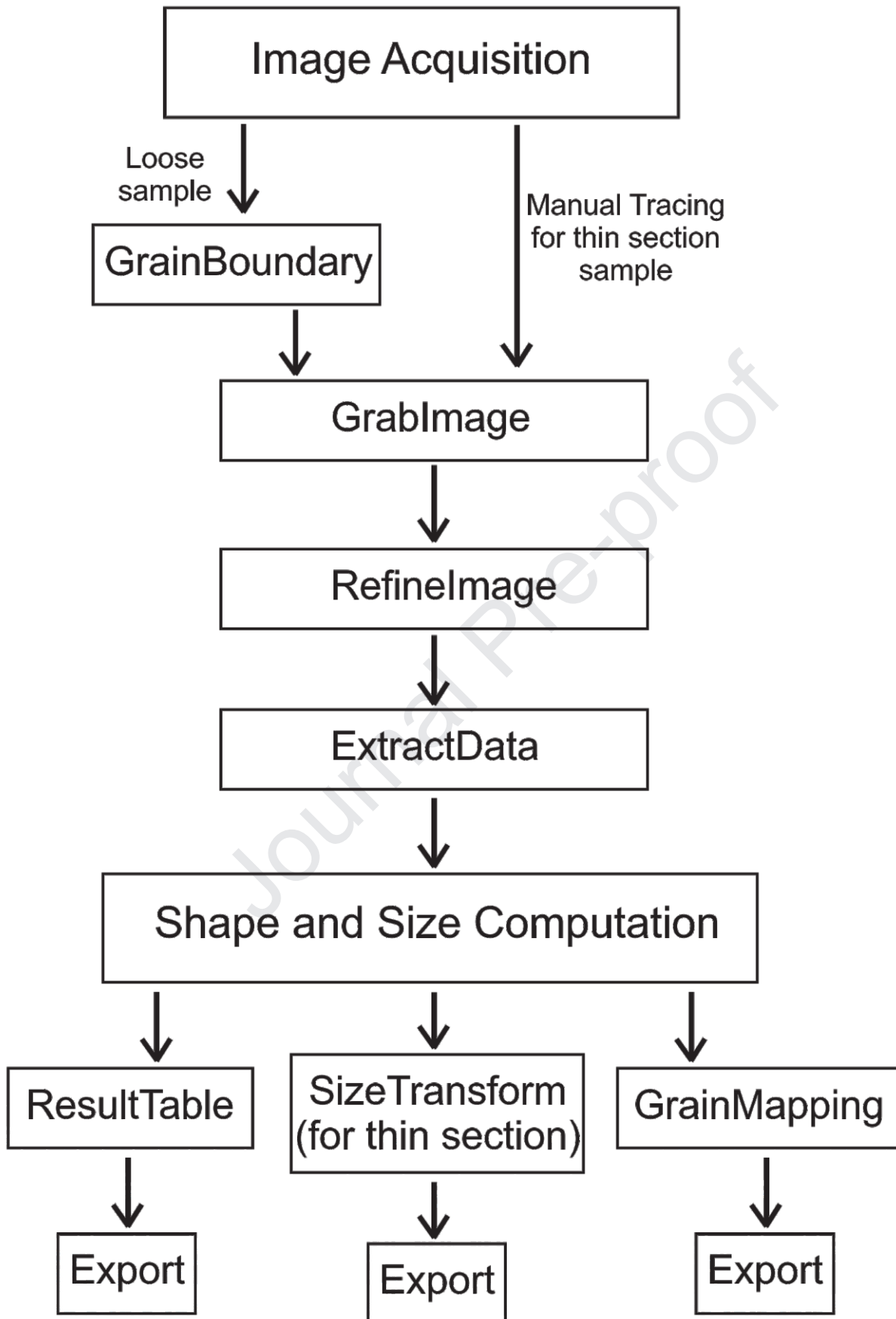
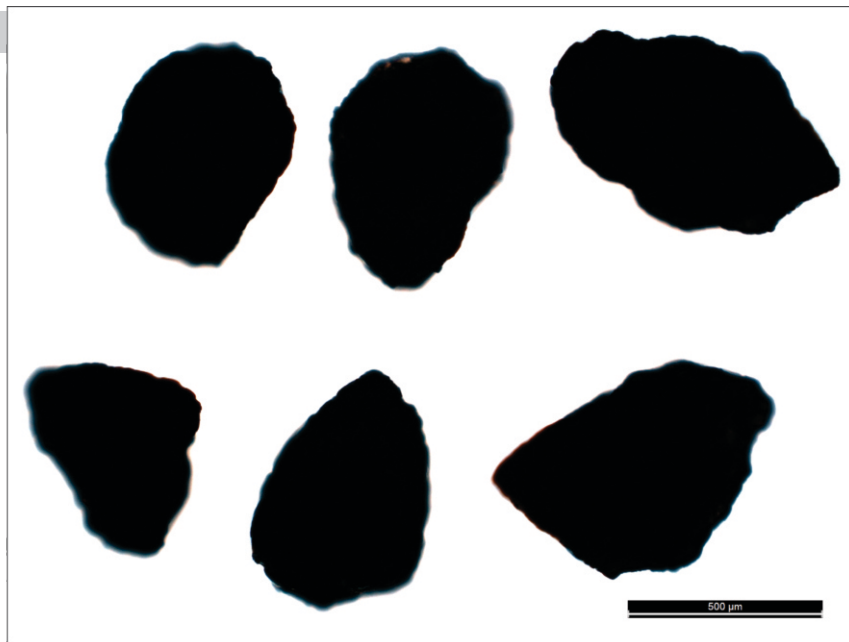
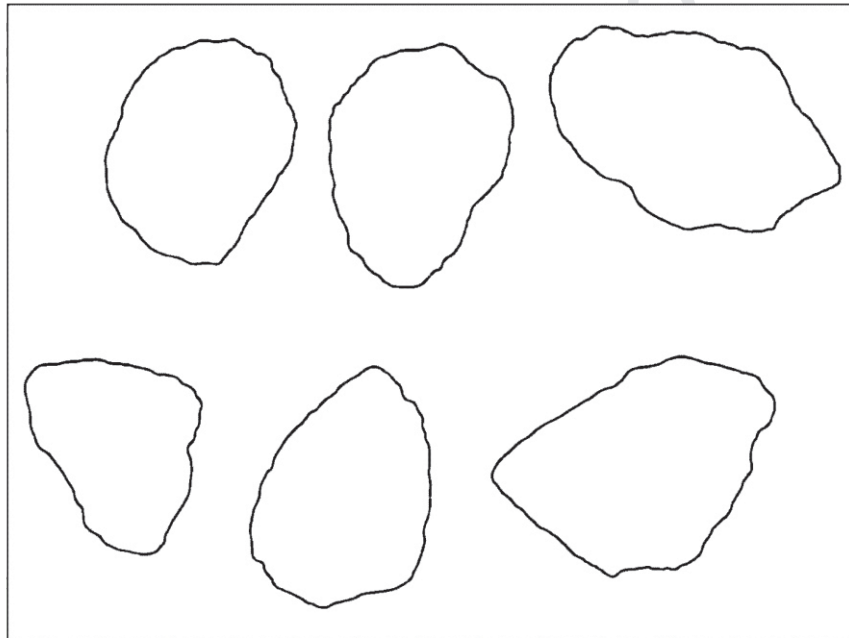


Figure 1

(A)



(B)

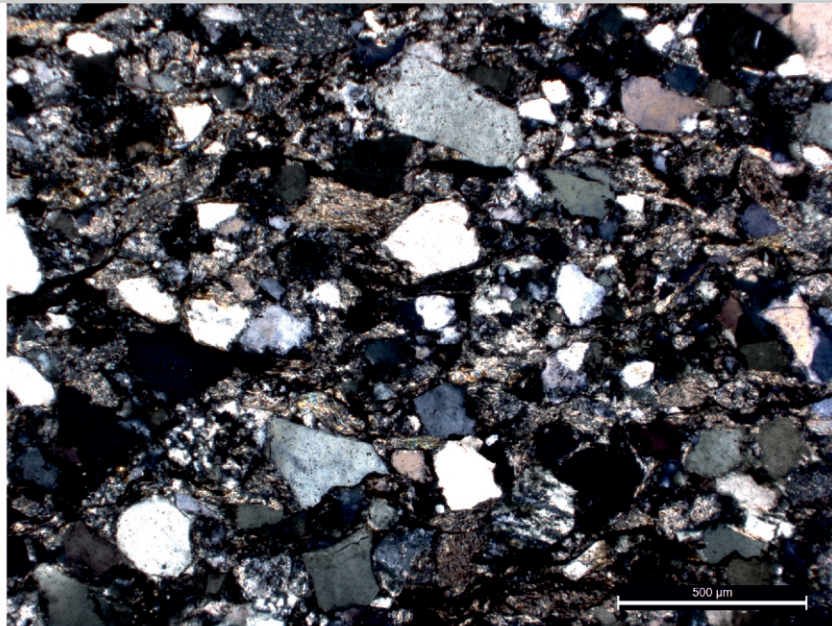


(C)

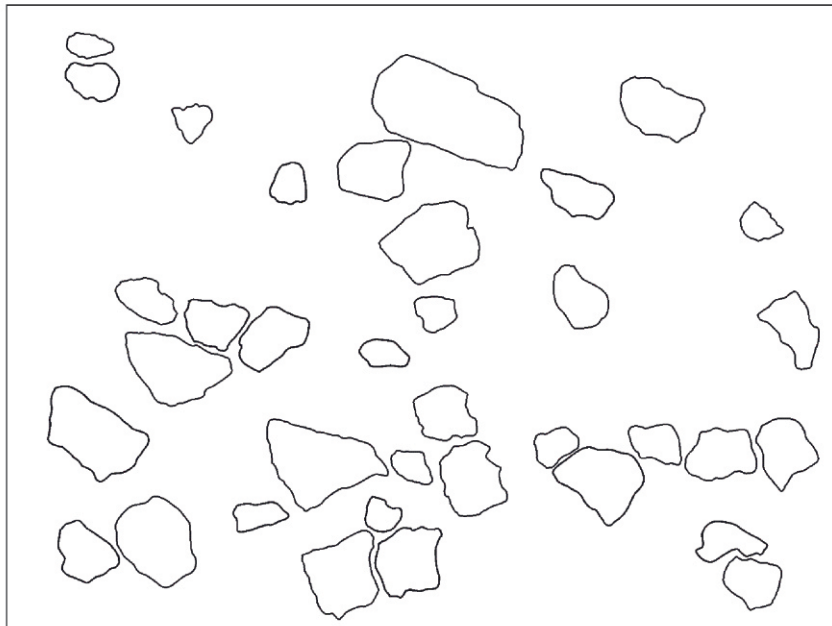


Figure 2

(A)



(B)



(C)

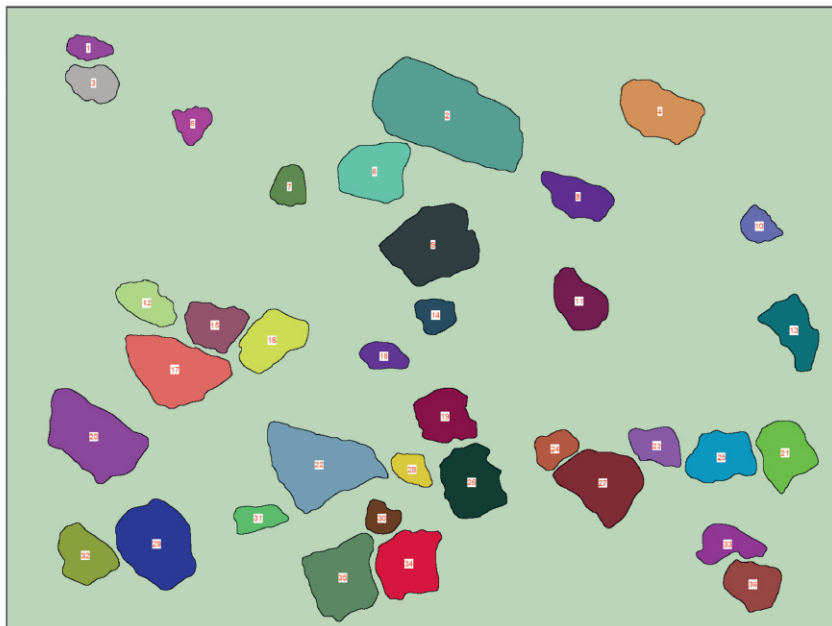
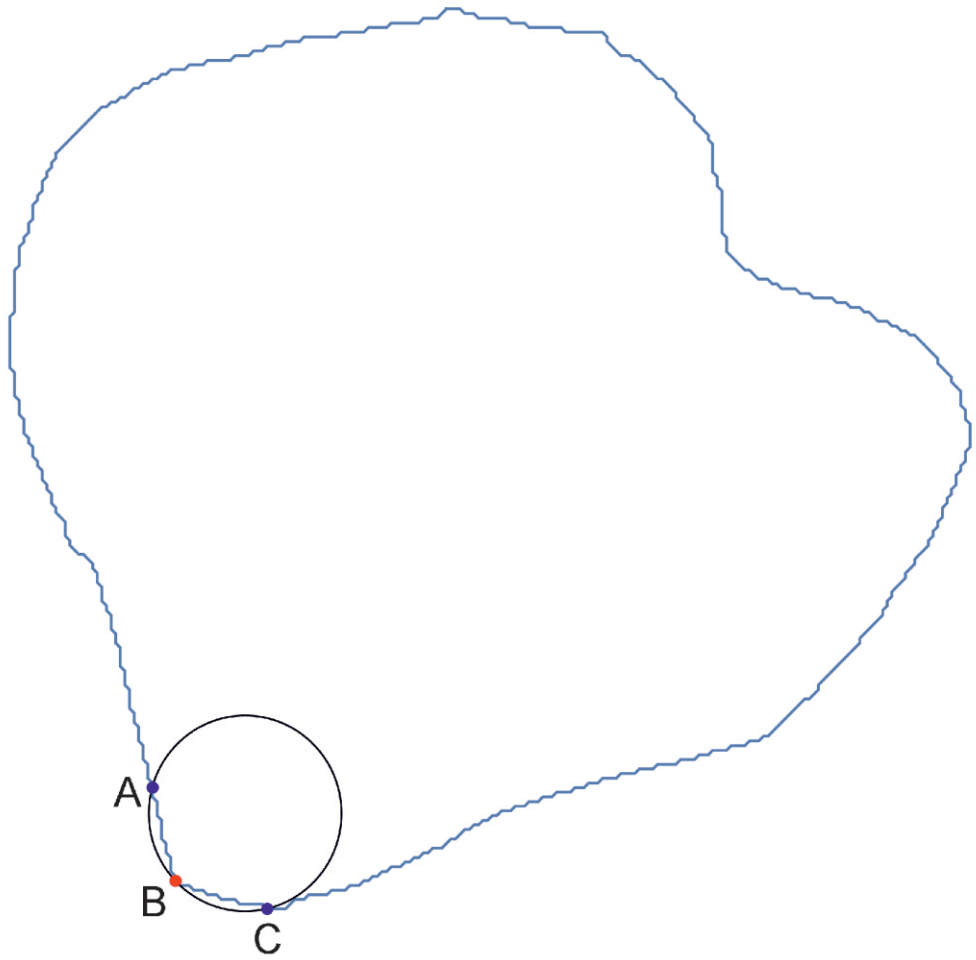


Figure 3

(A)



(B)

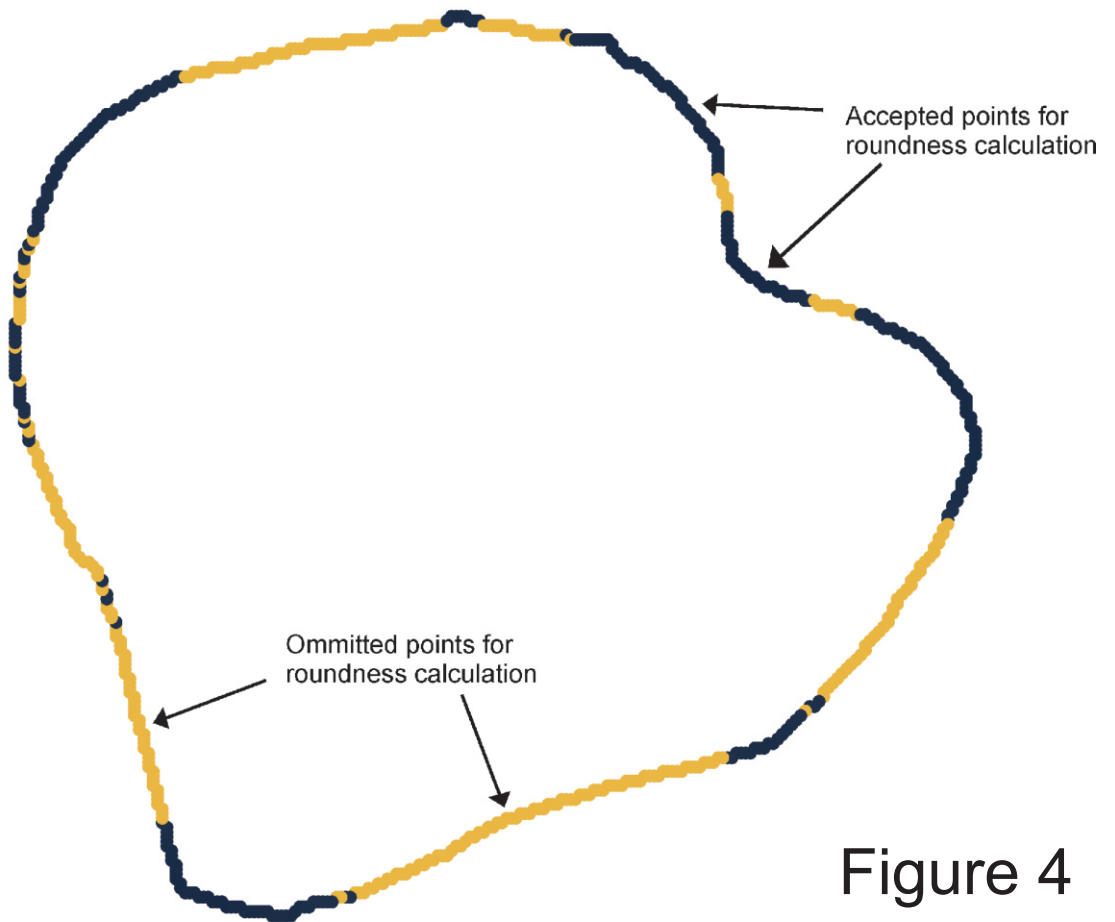


Figure 4

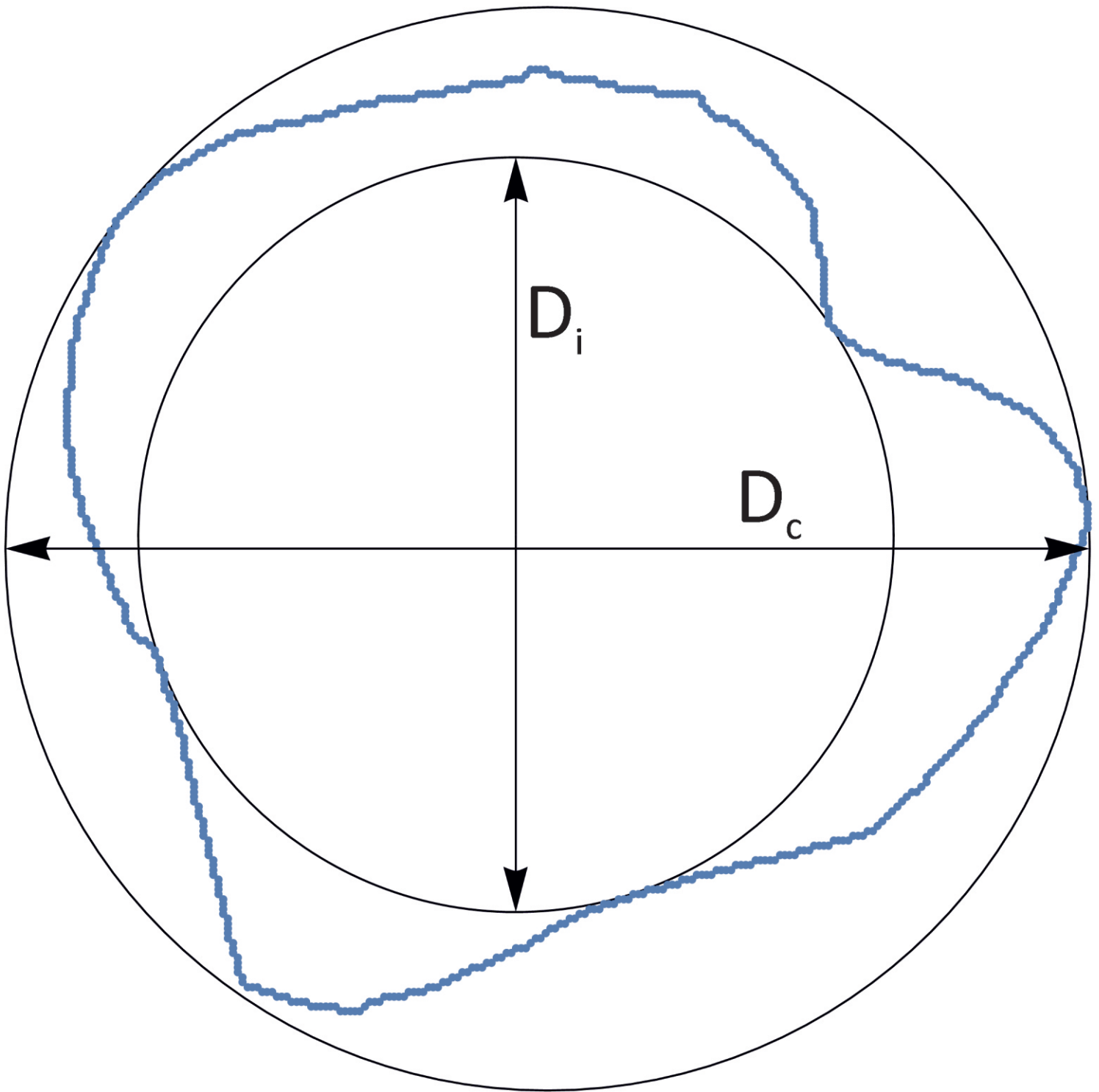
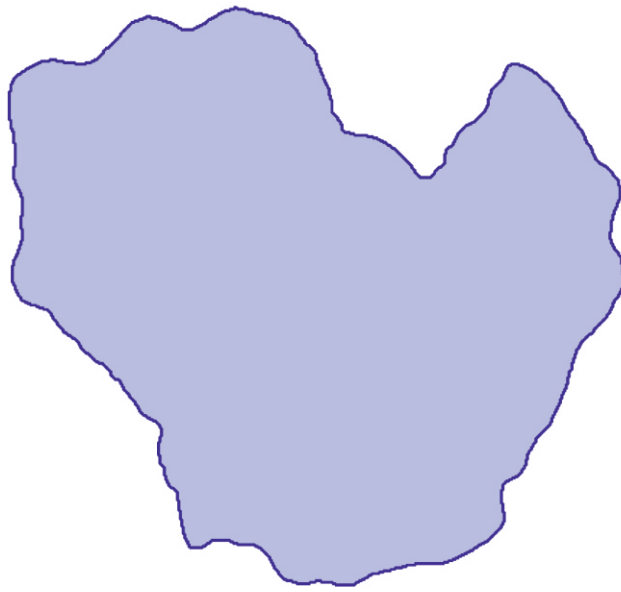
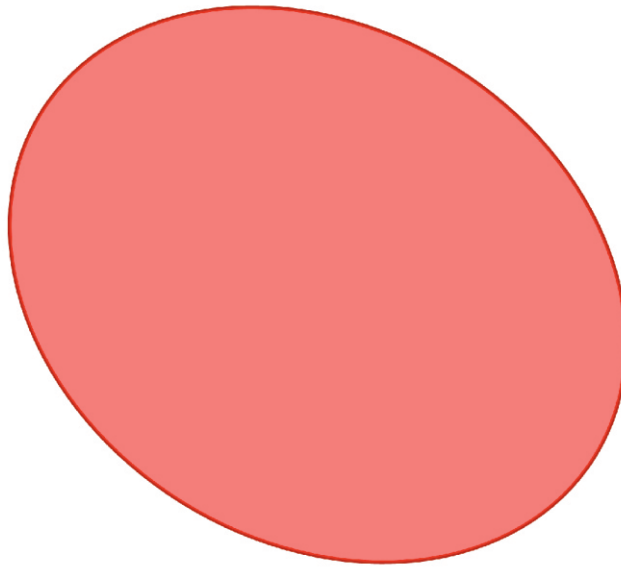


Figure 5

(A)



(B)



(C)

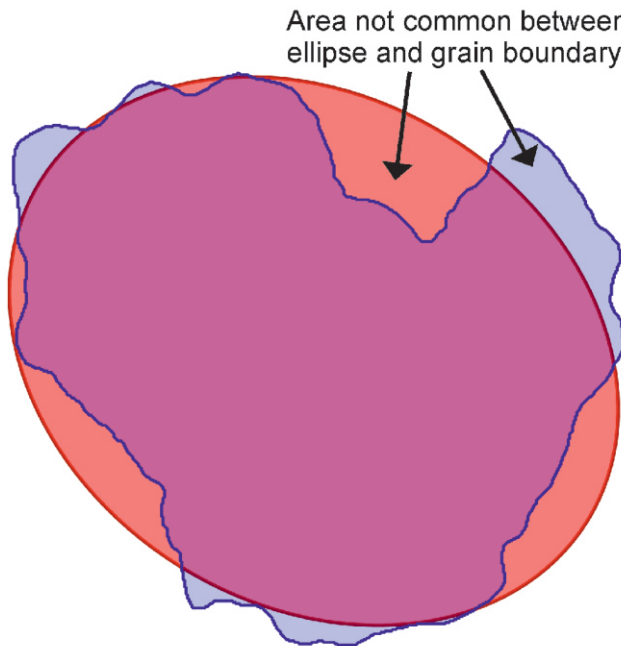


Figure 6

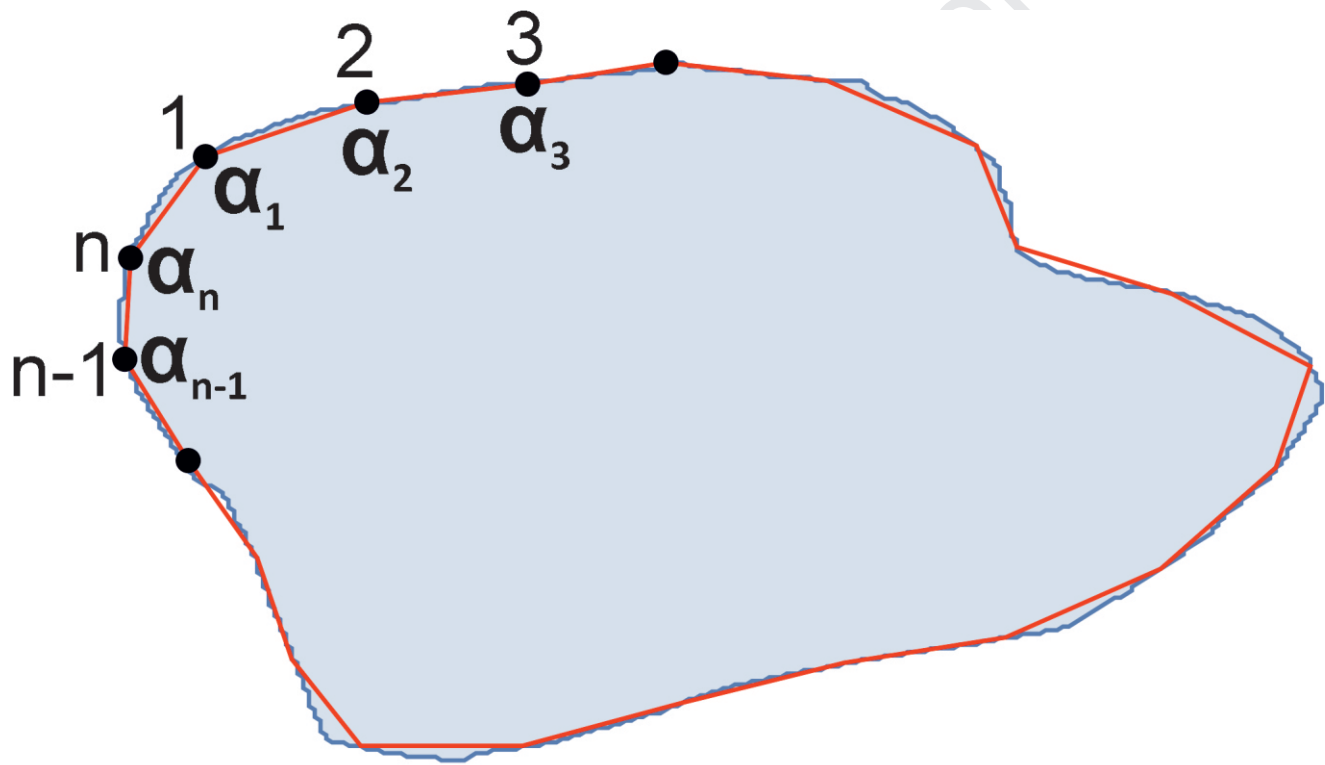


Figure 7

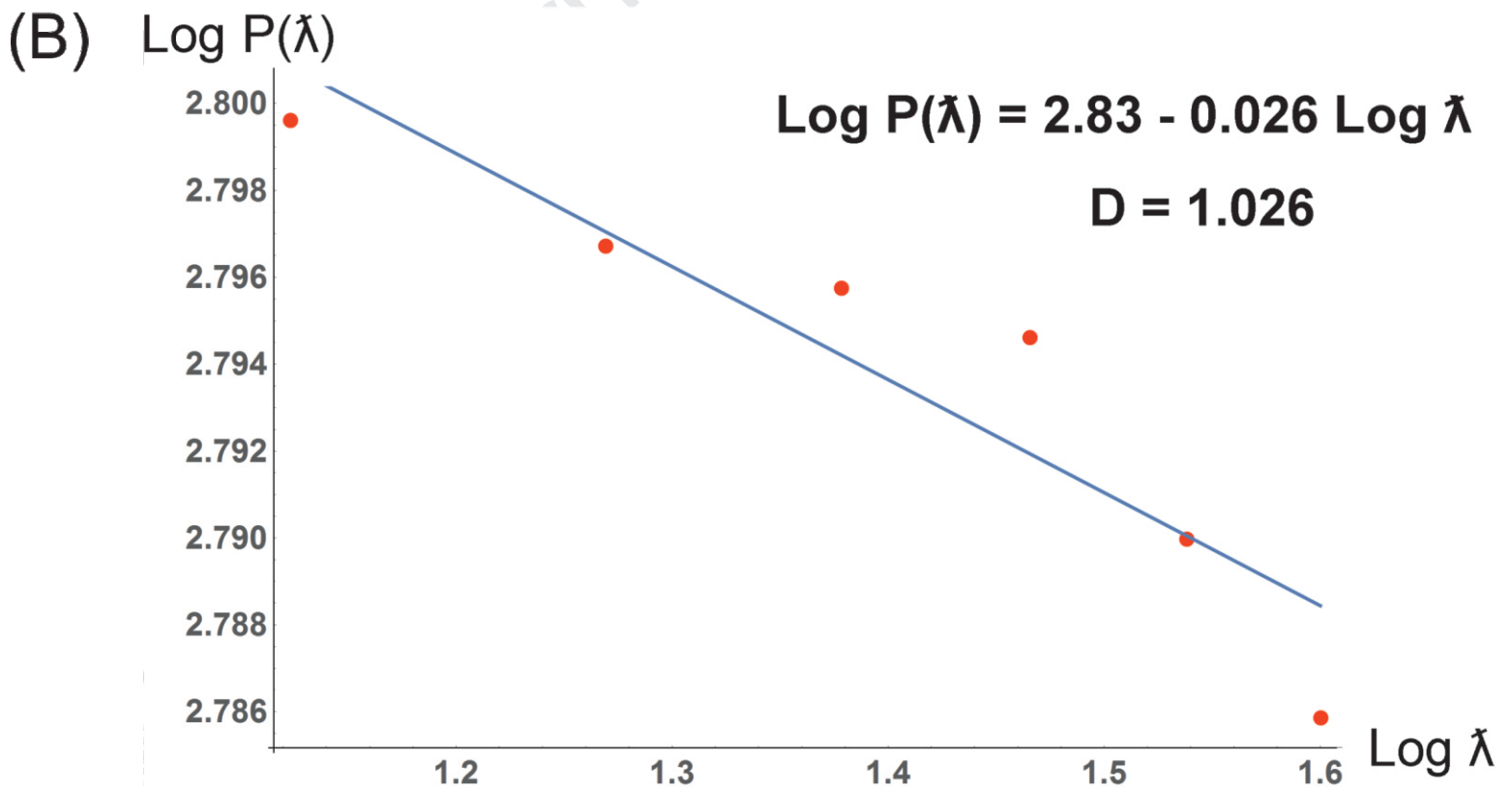
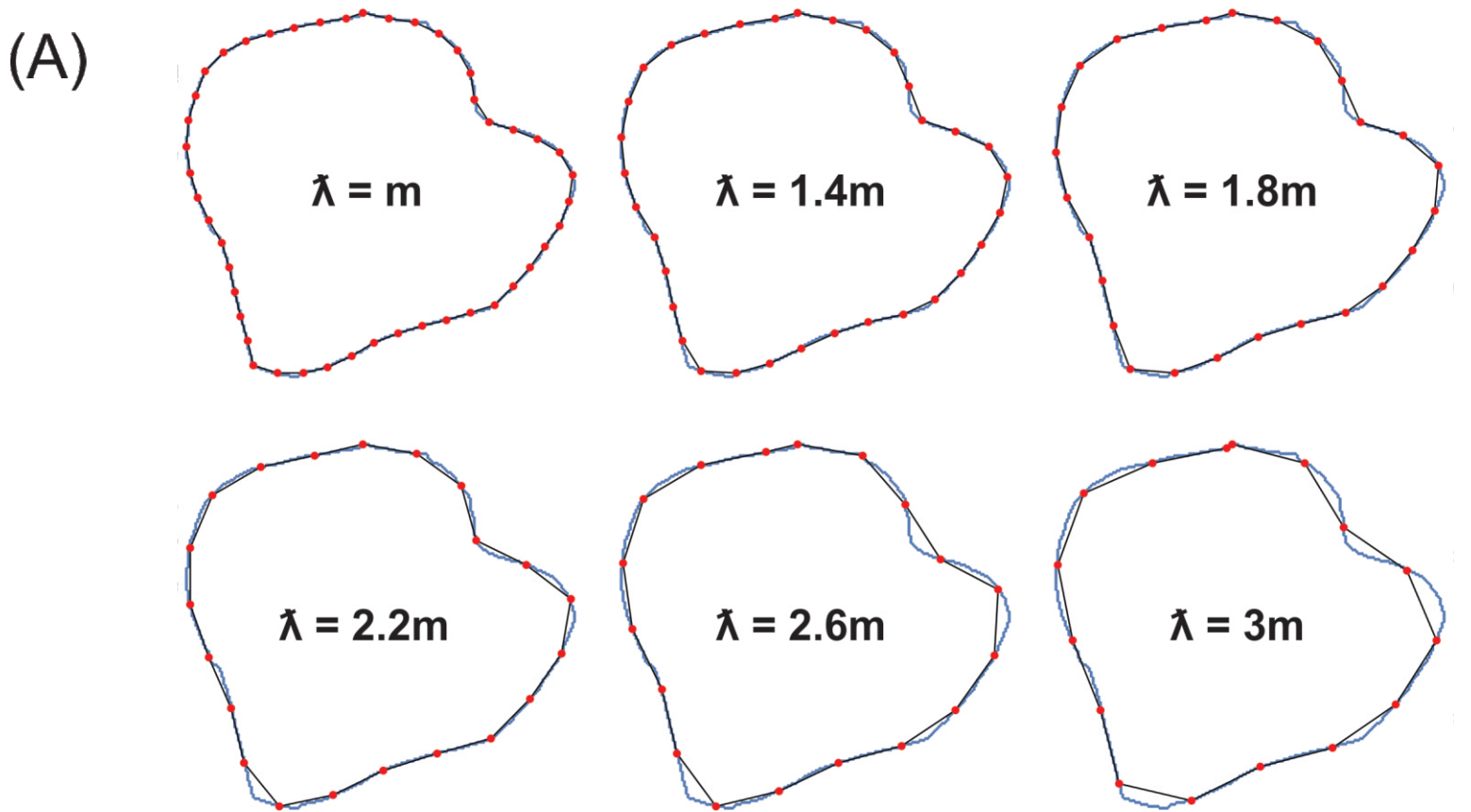


Figure 8

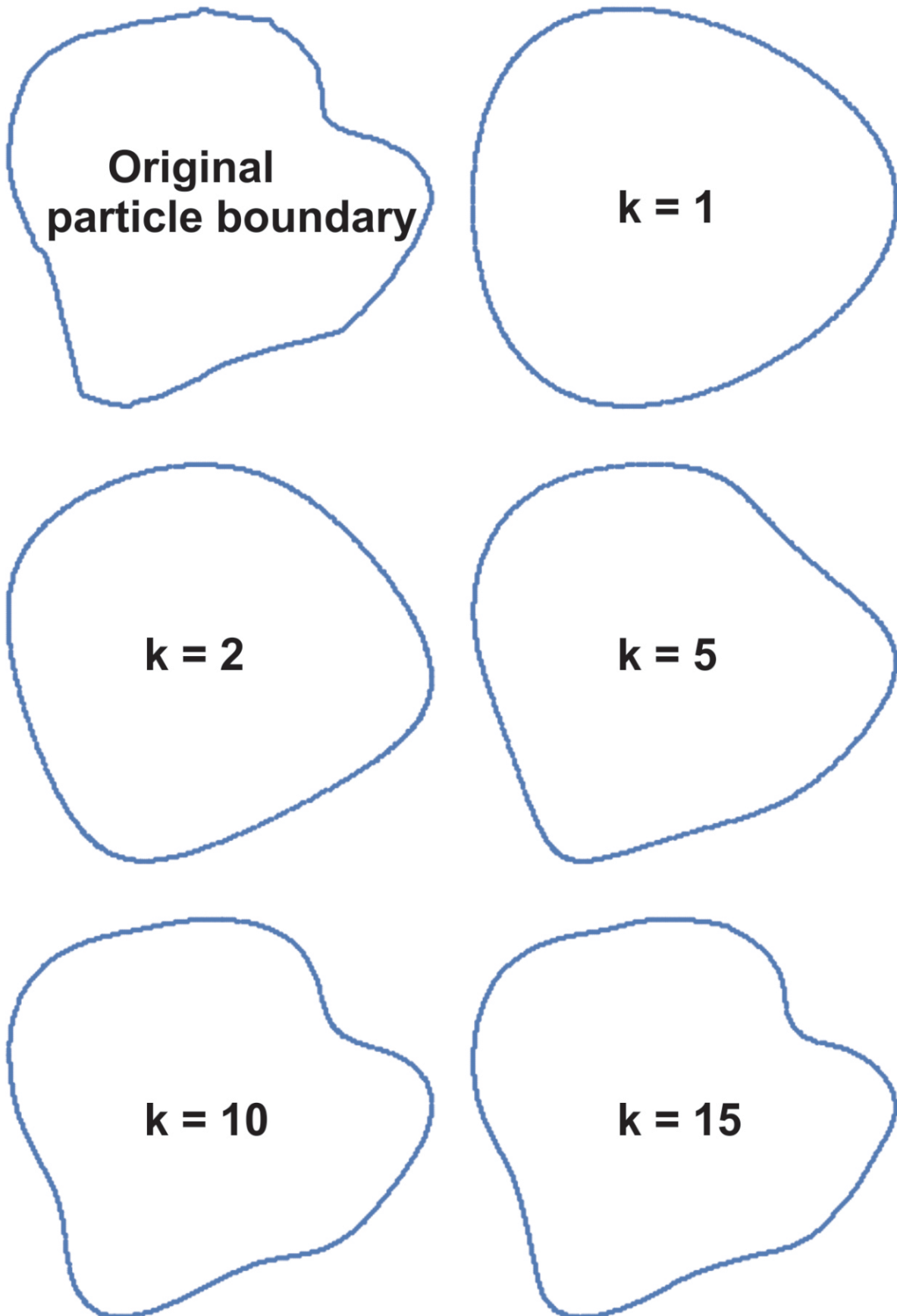


Figure 9

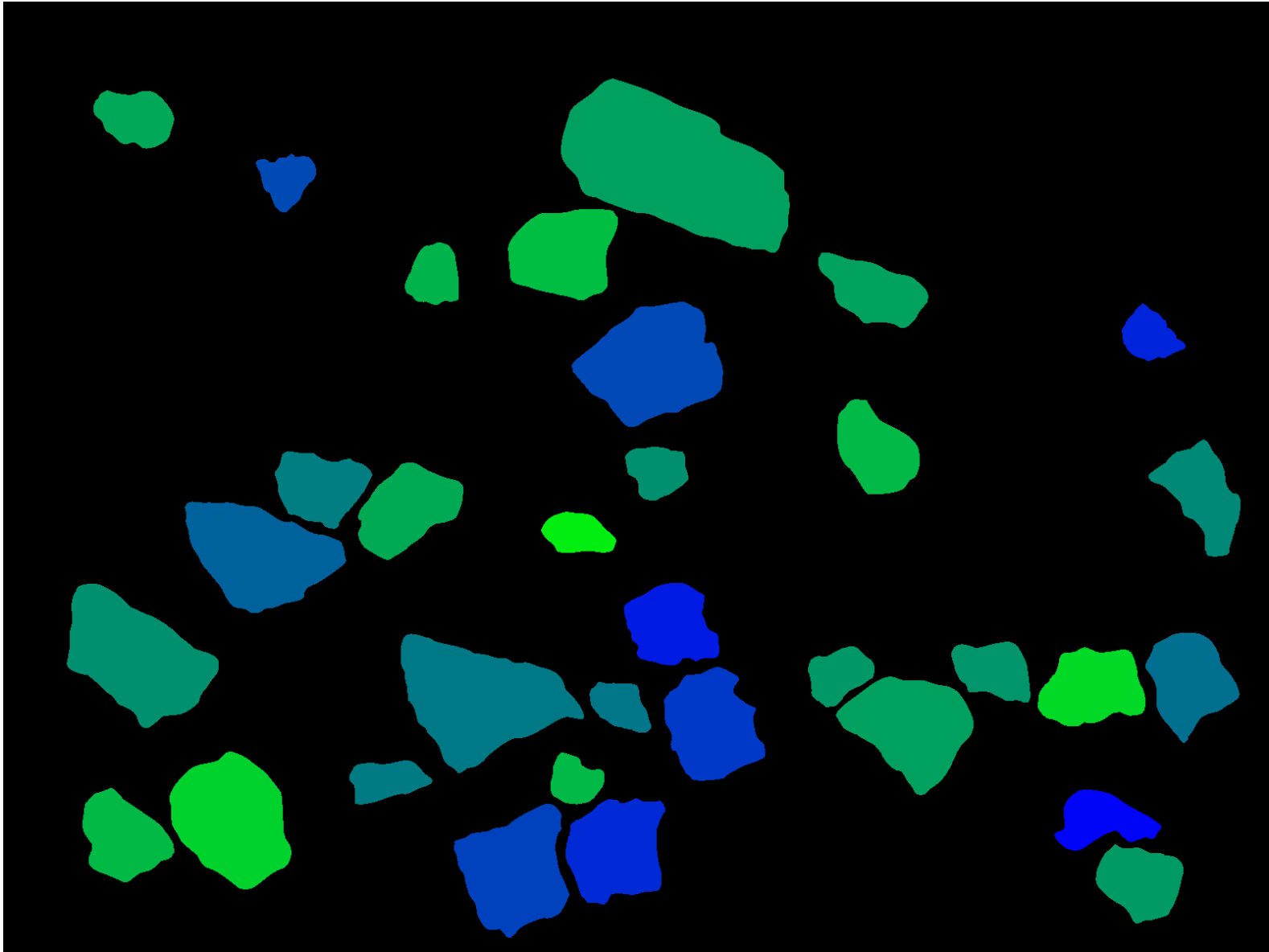


Figure 10

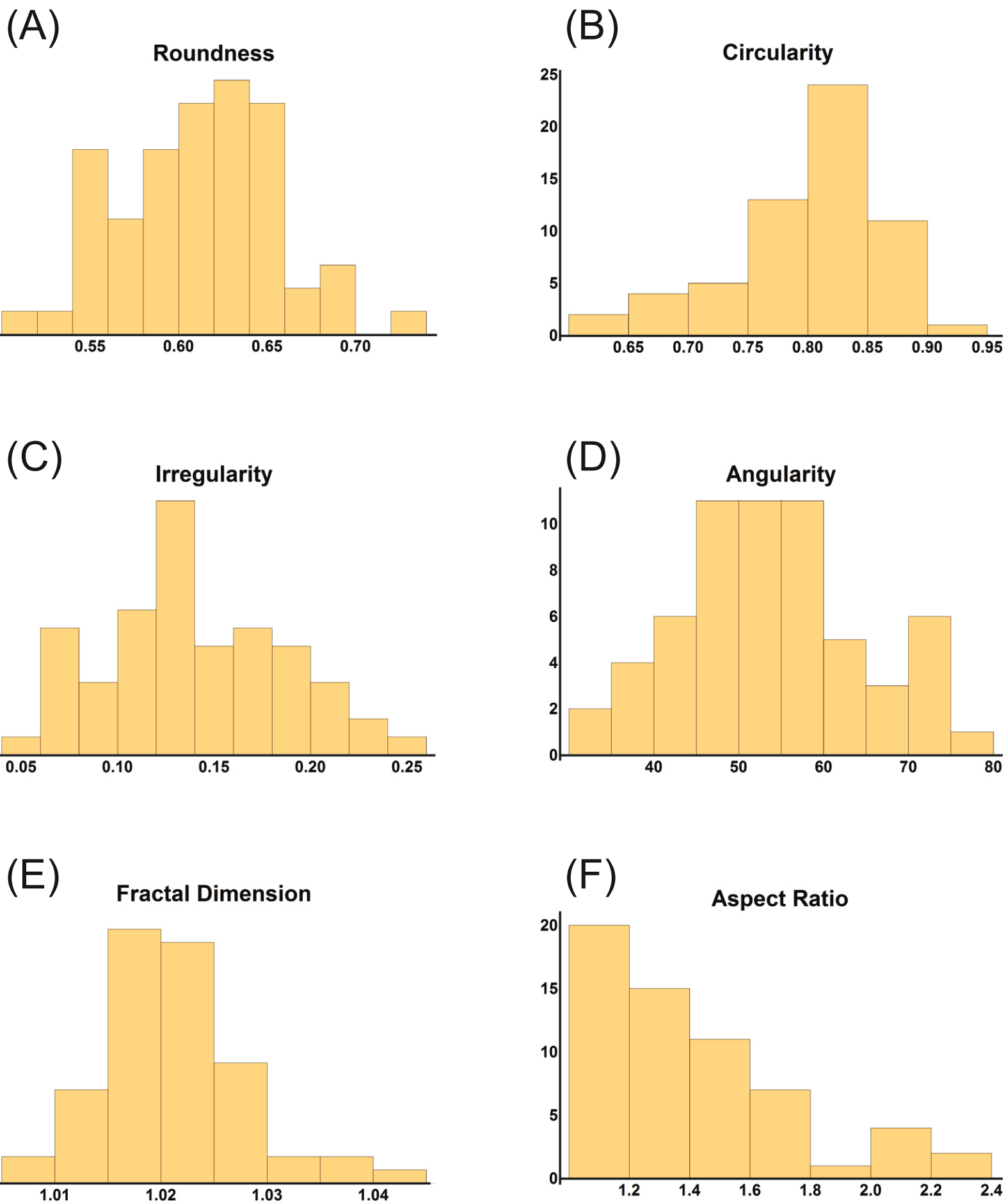


Figure 11

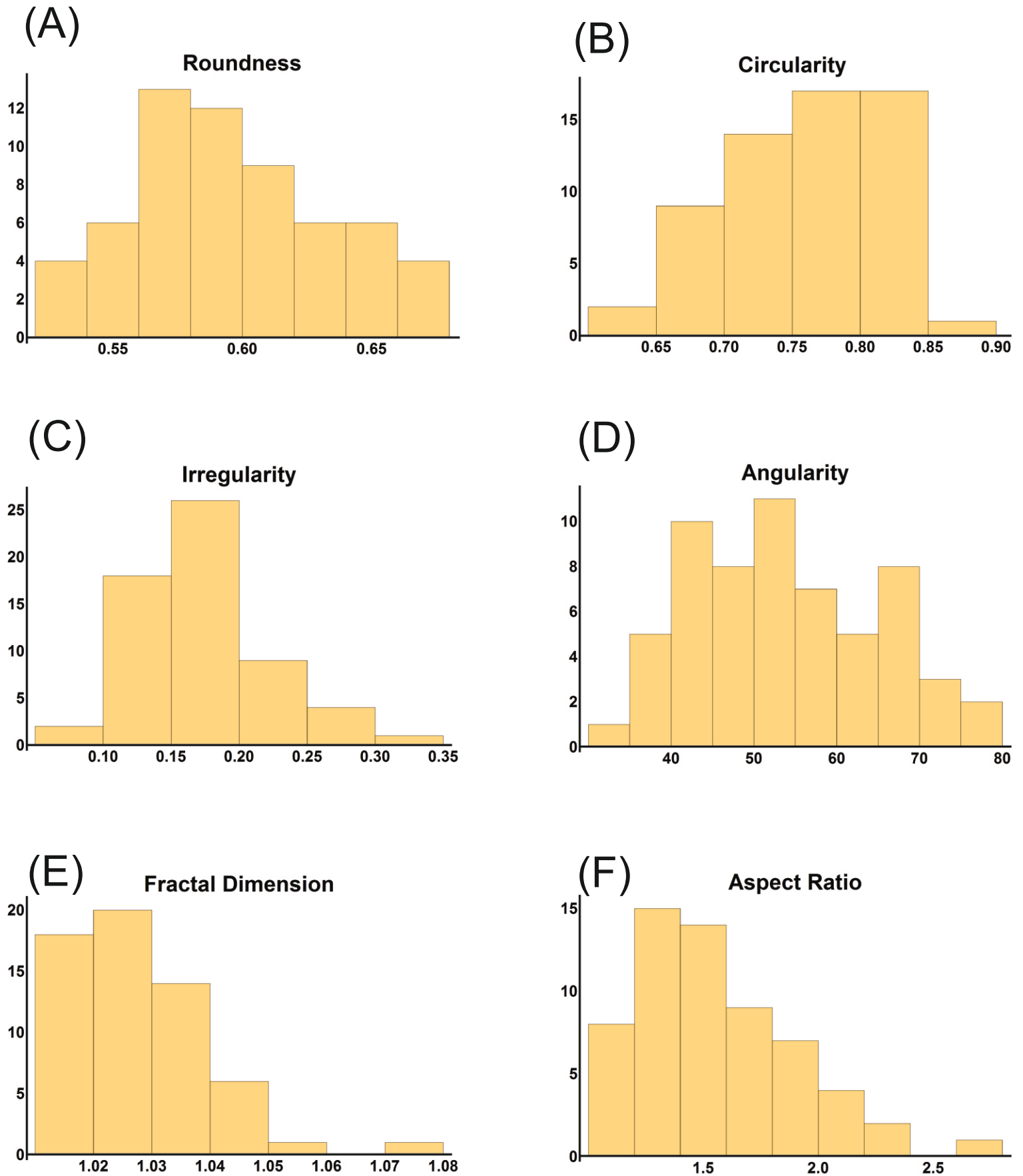


Figure 12

Conflict of Interest statement

Date: 26-09-2019

Manuscript Code: CAGEO_2019_508

Manuscript Title: Image based Particle Shape Analysis Toolbox (IPSAT)

The authors listed below certify that they have NO affiliations with or involvement in any organisation or entity with any financial interest (such as honoraria; educational grants; participation in speakers' bureaus; membership, employment, consultancies, stock ownership, or other equity interest; and expert testimony or patent-licensing arrangements), or non-financial interest (such as personal or professional relationships, affiliations, knowledge or beliefs) in the subject matter or materials discussed in this manuscript.

Authors names:

Mohit Tunwal

Kieran F. Mulchrone

Patrick A. Meere